IL NUOVO CIMENTO VOL. 3 C, N. 3 Maggio-Giugno 1980

Analogical Device for a Rough Localization of Gravitational-Wave Sources.

S. FRASCA

Istituto di Fisica dell'Università - Roma, Italia

(ricevuto il 22 Aprile 1980)

Summary. — The response of a gravitational cilindrical antenna depends, besides on the values of the intensity of the wave and the sensitivity of the antenna, on the angle between the direction of the source and the axis of the antenna and on the polarization angle of the wave. In this paper a device (gravitational astrolabe) that can roughly compute the angular part of the response is presented. It gives the zone of the sky toward which a given antenna is « directed » at a certain time, the angle of polarization that is best « received » and solves easily a number of similar problems.

1. – Introduction.

The problem of localizing on the sky the sources of gravitational waves can be solved by measuring with adequate accuracy the time of arrival of the same signal at three (or more) distant stations arranged to form a very-long-base interferometer. Most probably many years have to pass before the detector technique reaches such an advanced stage. In the meantime the localization of g.w. (gravitational wave) sources can be made by methods that will be described in a forthcoming paper.

This approach is based on a detailed analysis of the constraints imposed by the radiation pattern of a single detector to both the position on the sky of a point source and the polarization of the corresponding radiation. This « geometric approach » unavoidably has a rather poor resolution, also because of the low signal-to-noise ratio (SNR) of any g.w. detector. As will appear in the following, it can still turn out very useful.

This paper contains the first step in this direction (1), *i.e.* a rough estimate of certain parameters of the source (celestial co-ordinates and polarization) that can be obtained by means of a simple analogic device, *the gravitational astrolabe*, in the case of a single detector. The discussion is carried on for a *cylindrical resonant antenna* (CRA), which is the kind of detector most widely used today (2). As will appear below, the same device can be used also for any other type of g.w. detector, by simply redesigning the lines drawn on its transparent overlay discs (*c*) in subsect. **2**˙1) according to the corresponding radiation and polarization patterns.

We consider a gravitational wave propagating in the direction $\hat{w}$ with a Fourier component at the same angular frequency ω of the CRA. The direction $\hat{w}$ forms the angle ϑ with the direction $\hat{z}$ of the CRA's axis (fig. 1)

$$\hat{w}\cdot\hat{z} = \cos\vartheta \,. \tag{1a}$$

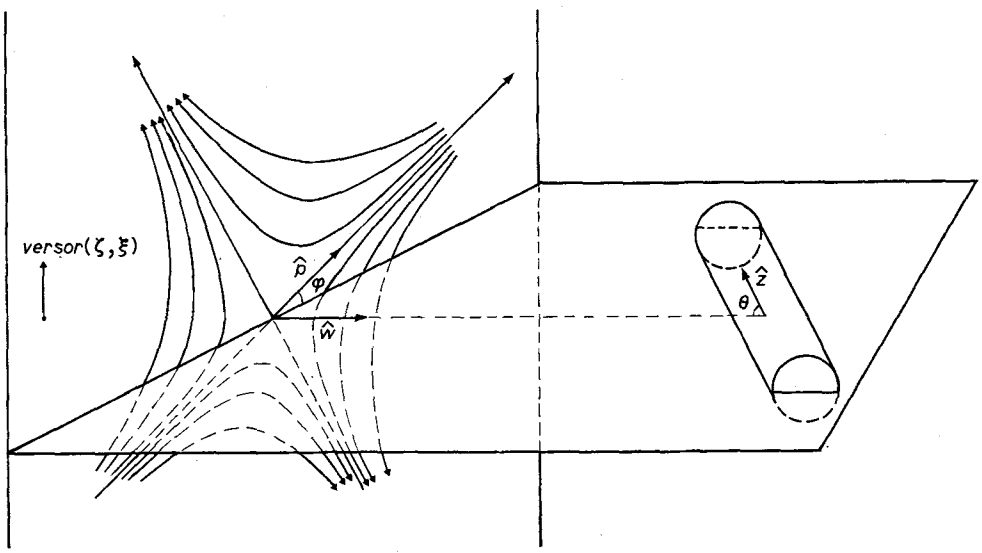

Fig. 1. – Interaction between the gravitational wave and a cylindrical antenna (see the text).

The wave can be either unpolarized or linearly polarized with one of the asymptotic lines of its lines of force in the direction $\hat{p}$ ($\hat{p}\cdot\hat{w} = 0$), which forms the angle φ with the plane defined by $\hat{w}$ and $\hat{z}$:

$$\frac{\hat{p}\cdot\hat{w}\times\hat{z}}{|\hat{w}\times\hat{z}|} = \sin\varphi \,. \tag{1b}$$

(1) The first to take this problem along similar lines was NITTI of this laboratory.
(2) E. AMALDI and G. PIZZELLA: *The search for gravitational waves*, in *Relativity, Quanta and Cosmology in the Development of the Scientific Thought of Albert Einstein* (New York, N. Y., 1979).

The most general state of polarization of a g.w. can always be decomposed into two parts, one polarized (*i.e.* of this type), the other unpolarized.

For the radiation and polarization pattern of the CRA we adopt the CRA's cross-section which, for a wave with the fraction ε of the energy in its linearly polarized part, can be written in the form

$$\sigma(\vartheta, \varphi, \varepsilon) = \sigma_{g.w.} f(\varepsilon, \varphi) \sin^4 \vartheta \,, \tag{2a}$$

where

$$f(\varepsilon, \varphi) = \tfrac{1}{2}(1 - \varepsilon) + \varepsilon \cos^2 2\varphi \tag{2b}$$

and

$$\sigma_{g.w.} = \frac{8}{\pi} \frac{G}{c} \left(\frac{v_s}{c}\right)^2 M \tag{2c}$$

is the maximum value of the cross-section corresponding to $\varepsilon = 1$, $\varphi = 0$, $\vartheta = 90°$.

Expressions (2*a*) and (2*b*) are conveniently cast in the form

$$\sigma(\vartheta, \varphi, \varepsilon) = \sigma_{g.w.} \left(\frac{1 - \varepsilon}{2} \sin^4 \vartheta + \varepsilon \cdot \sin^4 \vartheta \cdot \cos^2 2\varphi \right), \tag{3}$$

which shows the different dependence of the CRA's cross-section on the variables ϑ, ε, φ for unpolarized and linearly polarized radiation.

In table I, I have collected for comparison the angular resolution Δr as well as the number N of resolved points on the whole celestial sphere for detectors of different types of radiation. As appears from expression (2), for

TABLE I.

	Δr	N	Note
Optical astronomy	0.02″ (Mount Palomar)	$4.25 \cdot 10^{14}$	
Radio astronomy	2′ (Arecibo, 21 cm)	$1.18 \cdot 10^{7}$	radiotelescope
	0.01″ (Intercontinental Net)	$1.70 \cdot 10^{15}$	long-base interferometer
Gravitational astronomy	30° (single antenna)	2	circular zone (see the text)
	10° (net)	66	ambiguity (see the text)
Gravitational astrolabe	1°	6600	ambiguity (see the text)
Human sight	2′	10^7	

fixed values of ε and φ, the angular resolution Δr of a CRA is the angular width of a circular zone of the sky. In all other cases listed in table I, Δr represents the linear dimensions of a spot. Furthermore, the information provided by a single CRA always contains an ambiguity between two opposite spots on the sky, which will be eliminated in the case of a set of CRA's, only when the time of arrival of the same signal will be measured with adequate resolution at a few stations. As a consequence of this ambiguity a CRA or a set of CRA's *sees* the northern and the southern celestial emisphere superimposed to each other.

The use of a gravitational astrolabe for providing the solution of a number of problems is justified by two types of considerations: 1) the angular resolution of any reasonable set of CRA's is always rather low, and 2) the dependence of the radiation and polarization pattern (2) on the variables ϑ and φ is rather involved, as can be seen by expressing the angular factor

$$F = \sin^4\vartheta \cdot \cos^2 2\varphi = \eta_\vartheta \cdot \eta_\varphi \tag{4}$$

in terms of the celestial co-ordinates of the source, the geographic co-ordinates of the CRA and Universal Time ([3]):

$$\begin{cases} F = (2X^2 + Y^2 - 1)^2, \\ X = \sin\delta_w \cdot \cos\psi[\sin(\mathrm{lat}) \cdot \cos H \cdot \cos\varrho - \sin\varrho \cdot \sin H] + \\ \quad + \sin\psi \cdot [\sin(\mathrm{lat}) \cdot \sin H \cdot \cos\varrho + \sin\varrho \cdot \cos H] + \cos\psi \cdot \cos(\mathrm{lat}) \cdot \cos\delta_w, \\ Y = \cos\delta_w[\cos\varrho \cdot \cos H \cdot \sin(\mathrm{lat}) - \sin\varrho \cdot \sin H] - \sin\delta_w \cdot \cos\varrho \cdot \cos(\mathrm{lat}). \end{cases} \tag{5}$$

The simple device described below does not replace these exact but complex formulae, which should be used in any final analysis. The astrolabe is designed only for providing a quick and intuitive first help in solving a number of problems. It provides two kinds of information:

1) For unpolarized radiation, it gives the zone of the sky from which g.w. sources are received, by the CRA at a certain time, with an intensity reduced with respect to its maximum response by the factor

$$\eta_\vartheta = \sin^4\vartheta \tag{6}$$

in certain preassigned ranges

$$1 \geqslant \eta_\vartheta \geqslant \tfrac{1}{2}, \qquad \tfrac{1}{2} \geqslant \eta_\vartheta \geqslant \tfrac{1}{4}, \qquad \tfrac{1}{4} \geqslant \eta_\vartheta. \tag{7}$$

([3]) J. A. TYSON and D. H. DOUGLASS: *Phys. Rev. Lett.*, **28**, 991 (1972).

2) For linearly polarized radiation, it gives the ranges of values of φ for which a source in a certain zone of the sky is best received. A possible and significant choice for the bounds of the ranges of φ values is

$$0^\circ, \quad 22.5^\circ, \quad 45^\circ, \quad 67.5^\circ, \tag{8}$$

corresponding to

$$\eta_\varphi = \cos^2 2\varphi = 1, \ \tfrac{1}{2}, \ 0, \ \tfrac{1}{2}. \tag{9}$$

The bounds (6) and (9) have a very simple physical meaning. If E_w is the intensity (4) carried by the wave in the vicinity of the CRA and E_{us} is the intensity « usable » by the CRA, we have

$$\frac{E_{us}}{E_w} = \eta_\vartheta \tag{10}$$

for unpolarized waves,

$$\frac{E_{us}}{E_w} = \eta_\vartheta \cdot \eta_\varphi \tag{11}$$

for waves polarized linearly in the φ direction.

A few examples of the kind of problems that can be solved by the use of the gravitational astrolabe are the following:

a) determination of the orientation of a single CRA which allows the contemporary reception of signals emitted by sources located in different parts of the sky (for example, the centre of our galaxy, Andromeda, Magellanic clouds, etc.),

b) determination of the orientation of a single CRA which allows the best possible distinction between two sources located in different parts of the sky,

c) determination of the orientation of a single CRA which allows the reception of the signals of a given source in a certain part of the year during the most favourable period of the day (for example, during the night, because of local disturbances),

d) choice of the orientation of the CRAs of different stations for the simultaneous detection of a given source,

e) choice of the orientation of a few antennas for the identification of the polarization state of a given source.

---

(4) The expression intensity has here a different meaning for periodic and burst sources. For periodic sources E_w is a *power density* (erg/s cm^2), for burst of radiation E_w is a *spectral energy* (erg/Hz cm^2).

In sect. **2** we describe the astrolabe and give a simple example of its use; in sect. **3** we describe its construction.

2. – The gravitational astrolabe.

2'1. *Description of the instrument.* – The astrolabe consists of (at least) four parts (fig. 2) and two formulae (see table II):

a) A *base* with a circular map of the sky with the northern and southern emisphere superimposed, because of the ambiguity already mentioned in sect. **1**. The North (and South) pole is at the centre. The map is obtained by stereographic projection (see fig. 3).

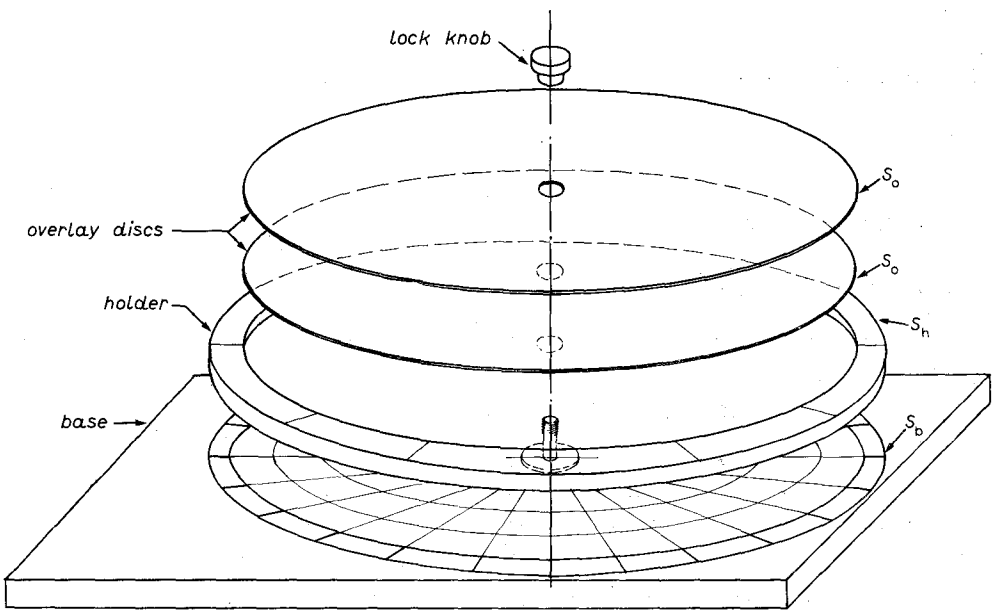

Fig. 2. – Scheme of the gravitational astrolabe, exploded view.

The circular scale (S_b) around the map gives the right ascension α (in hours). The net of parallels and meridians divides the emisphere in 97 sectors, which will turn out very useful for the study of gravitational-wave sources by means of a set of stations.

The location of a few presumable g.w. sources is also shown on the map.

b) A disc, the *holder*, made of transparent rigid plastic, which can rotate around a pivot placed at the centre of the map (pole). Its edge is graduated (scale S_h) in months (12) and days (365).

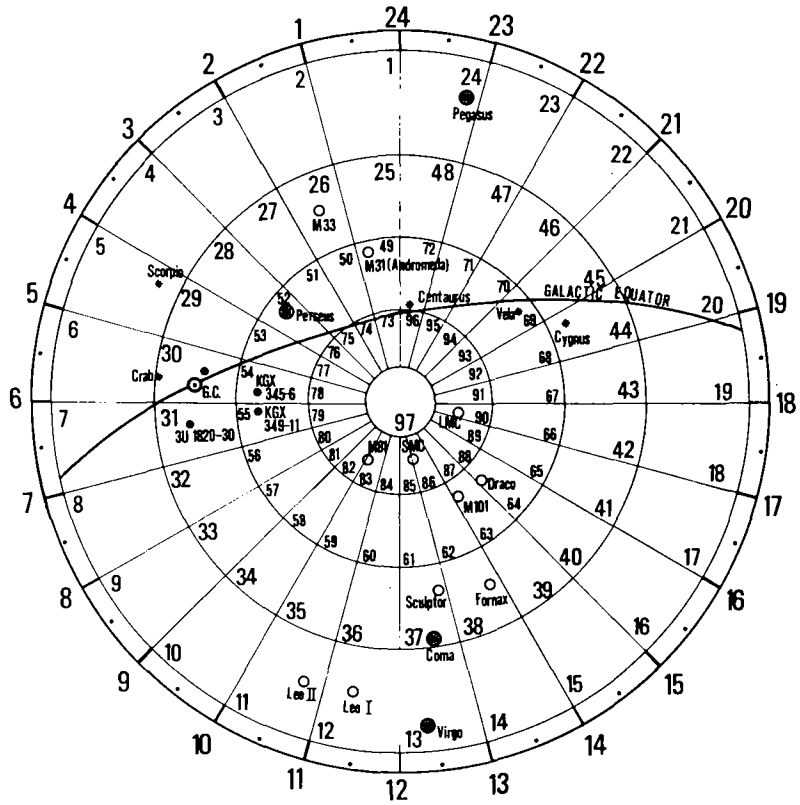

Fig. 3. – The sky map for the gravitational astrolabe. Around the map is the scale S_b, in hours (see the text). * X-ray binaries or pulsars, • globular clusters, o galaxies and systems, ⊙ centre of our galaxy, ⓞ clusters of galaxies.

c) A few thin and transparent *overlay discs*, which can be interchanged and/or superimposed. They are different for different values of the declination δ_a of the axis of the CRA, but independent of UT (Universal Time) and α_a (right ascension).

A few lines are drawn on each overlay (disc) which are of two types (see fig. 4-8).

c_1) *Radiation pattern overlay* (RPO) with lines of equation

$$\eta_\vartheta = \sin^4 \vartheta = \text{const} \tag{12a}$$

with

$$\eta_\vartheta = 1\,,\ \tfrac{1}{2}\,,\ \tfrac{1}{4} \tag{12b}$$

TABLE II. – *Antenna orientation.* Values of the declination (first row) and of the right ascension angle of the CRA axis (horizontal scale).

	0	5	10	15	20	25	30	35	40
−90	0	0	0	0	0	0	0	0	0
	Sep. 23	Sep. 28	Oct. 3	Oct. 8	Oct. 13	Oct. 18	Oct. 23	Oct. 28	Nov. 2
−85	5	5	5	5	5	5	4	4	4
	Sep. 23	Sep. 28	Oct. 3	Oct. 8	Oct. 13	Oct. 18	Oct. 23	Oct. 28	Nov. 2
−80	10	10	10	10	9	9	9	8	8
	Sep. 23	Sep. 28	Oct. 3	Oct. 8	Oct. 13	Oct. 18	Oct. 23	Oct. 28	Nov. 3
−75	15	15	15	14	14	14	13	12	11
	Sep. 23	Sep. 28	Oct. 3	Oct. 8	Oct. 13	Oct. 19	Oct. 24	Oct. 29	Nov. 3
−70	20	20	20	19	19	18	17	16	15
	Sep. 23	Sep. 28	Oct. 3	Oct. 9	Oct. 14	Oct. 19	Oct. 25	Oct. 30	Nov. 4
−65	25	25	25	24	23	23	21	20	19
	Sep. 23	Sep. 28	Oct. 4	Oct. 9	Oct. 15	Oct. 20	Oct. 25	Oct. 31	Nov. 5
−60	30	30	29	29	28	27	26	24	23
	Sep. 23	Sep. 28	Oct. 4	Oct. 10	Oct. 16	Oct. 21	Oct. 27	Nov. 1	Nov. 6
−55	35	35	34	34	33	31	30	28	26
	Sep. 23	Sep. 29	Oct. 5	Oct. 11	Oct. 17	Oct. 23	Oct. 28	Nov. 3	Nov. 8
−50	40	40	39	38	37	36	34	32	29
	Sep. 23	Sep. 29	Oct. 6	Oct. 12	Oct. 18	Oct. 24	Oct. 30	Nov. 5	Nov. 10
−45	45	45	44	43	42	40	38	35	33
	Sep. 24	Sep. 30	Oct. 7	Oct. 14	Oct. 20	Oct. 26	Nov. 1	Nov. 7	Nov. 12
−40	50	50	49	48	46	44	42	39	36
	Sep. 24	Sep. 30	Oct. 8	Oct. 15	Oct. 22	Oct. 29	Nov. 4	Nov. 10	Nov. 15
−35	55	55	54	52	50	48	45	42	39
	Sep. 24	Oct. 1	Oct. 10	Oct. 18	Oct. 25	Nov. 1	Nov. 7	Nov. 13	Nov. 18
−30	60	60	59	57	54	52	49	45	42
	Sep. 24	Oct. 3	Oct. 12	Oct. 21	Oct. 29	Nov. 5	Nov. 11	Nov. 17	Nov. 22
−25	65	65	63	61	58	55	52	48	44
	Sep. 24	Oct. 4	Oct. 15	Oct. 25	Nov. 3	Nov. 10	Nov. 16	Nov. 21	Nov. 26
−20	70	69	68	65	62	58	54	50	46
	Sep. 24	Oct. 7	Oct. 20	Oct. 31	Nov. 9	Nov. 16	Nov. 22	Nov. 26	Nov. 30
−15	75	74	72	69	65	61	57	52	48
	Sep. 24	Oct. 12	Oct. 27	Nov. 8	Nov. 17	Nov. 23	Nov. 28	Dec. 2	Dec. 5
−10	80	79	76	72	68	63	59	54	49
	Sep. 25	Oct. 20	Nov. 8	Nov. 19	Nov. 27	Dec. 2	Dec. 6	Dec. 9	Dec. 11
− 5	85	83	79	74	69	65	60	55	50
	Sep. 26	Nov. 7	Nov. 26	Dec. 4	Dec. 9	Dec. 12	Dec. 14	Dec. 16	Dec. 17
0	90	85	80	75	70	65	60	55	50
	Dec. 23	Dec. 23	Dec. 23	Dec. 23	Dec. 23	Dec. 23	Dec. 23	Dec. 23	Dec. 23

(second row) of the CRA axis as a function of the station latitude (vertical scale) and the azimuthal

45	50	55	60	65	70	75	80	85	90
0	0	0	0	0	0	0	0	0	0
Nov. 7	Nov. 12	Nov. 17	Nov. 22	Nov. 27	Dec. 2	Dec. 8	Dec. 13	Dec. 18	Dec. 23
4	3	3	2	2	2	1	1	0	0
Nov. 7	Nov. 12	Nov. 17	Nov. 22	Nov. 27	Dec. 3	Dec. 8	Dec. 13	Dec. 18	Dec. 23
7	6	6	5	4	3	3	2	1	0
Nov. 8	Nov. 13	Nov. 18	Nov. 23	Nov. 28	Dec. 3	Dec. 8	Dec. 13	Dec. 18	Dec. 23
11	10	9	7	6	5	4	3	1	0
Nov. 8	Nov. 13	Nov. 18	Nov. 23	Nov. 28	Dec. 3	Dec. 8	Dec. 13	Dec. 18	Dec. 23
14	13	11	10	8	7	5	3	2	0
Nov. 9	Nov. 14	Nov. 19	Nov. 24	Nov. 29	Dec. 4	Dec. 8	Dec. 13	Dec. 18	Dec. 23
17	16	14	12	10	8	6	4	2	0
Nov. 10	Nov. 15	Nov. 20	Nov. 25	Nov. 30	Dec. 4	Dec. 9	Dec. 14	Dec. 18	Dec. 23
21	19	17	14	12	10	7	5	2	0
Nov. 11	Nov. 16	Nov. 21	Nov. 26	Nov. 30	Dec. 5	Dec. 10	Dec. 14	Dec. 18	Dec. 23
24	22	19	17	14	11	9	6	3	0
Nov. 13	Nov. 18	Nov. 23	Nov. 27	Dec. 2	Dec. 6	Dec. 10	Dec. 14	Dec. 19	Dec. 23
27	24	22	19	16	13	10	6	3	0
Nov. 15	Nov. 20	Nov. 24	Nov. 29	Dec. 3	Dec. 7	Dec. 11	Dec. 15	Dec. 19	Dec. 23
30	27	24	21	17	14	11	7	4	0
Nov. 17	Nov. 22	Nov. 26	Nov. 30	Dec. 4	Dec. 8	Dec. 12	Dec. 16	Dec. 19	Dec. 23
33	29	26	23	19	15	11	8	4	0
Nov. 20	Nov. 24	Nov. 28	Dec. 2	Dec. 6	Dec. 9	Dec. 13	Dec. 16	Dec. 19	Dec. 23
35	32	28	24	20	16	12	8	4	0
Nov. 23	Nov. 27	Dec. 1	Dec. 4	Dec. 8	Dec. 11	Dec. 14	Dec. 17	Dec. 20	Dec. 23
38	34	30	26	21	17	13	9	4	0
Nov. 26	Nov. 30	Dec. 3	Dec. 6	Dec. 9	Dec. 12	Dec. 15	Dec. 18	Dec. 20	Dec. 23
40	36	31	27	23	18	14	9	5	0
Nov. 30	Dec. 3	Dec. 6	Dec. 9	Dec. 11	Dec. 14	Dec. 16	Dec. 18	Dec. 21	Dec. 23
42	37	33	28	23	19	14	9	5	0
Dec. 4	Dec. 7	Dec. 9	Dec. 11	Dec. 14	Dec. 16	Dec. 17	Dec. 19	Dec. 21	Dec. 23
43	38	34	29	24	19	14	10	5	0
Dec. 8	Dec. 10	Dec. 12	Dec. 14	Dec. 16	Dec. 17	Dec. 19	Dec. 20	Dec. 21	Dec. 23
44	39	34	29	25	20	15	10	5	0
Dec. 13	Dec. 14	Dec. 16	Dec. 17	Dec. 18	Dec. 19	Dec. 20	Dec. 21	Dec. 22	Dec. 23
45	40	35	30	25	20	15	10	5	0
Dec. 18	Dec. 19	Dec. 19	Dec. 20	Dec. 20	Dec. 21	Dec. 21	Dec. 22	Dec. 22	Dec. 23
45	40	35	30	25	20	15	10	5	0
Dec. 23	Dec. 23	Dec. 23	Dec. 23	Dec. 23	Dec. 23	Dec. 23	Dec. 23	Dec. 23	Dec. 23

TABLE II (*continued*).

	0	5	10	15	20	25	30	35	40
5	85 Mar. 21	83 Feb. 6	79 Jan. 18	74 Jan. 10	69 Jan. 5	65 Jan. 2	60 Dec. 31	55 Dec. 30	50 Dec. 29
10	80 Mar. 22	79 Feb. 25	76 Feb. 6	72 Jan. 25	68 Jan. 18	63 Jan. 12	59 Jan. 9	54 Jan. 6	49 Jan. 4
15	75 Mar. 22	74 Mar. 5	72 Feb. 17	69 Feb. 5	65 Jan. 28	61 Jan. 21	57 Jan. 16	52 Jan. 12	48 Jan. 9
20	70 Mar. 22	69 Mar. 9	68 Feb. 24	65 Feb. 13	62 Feb. 5	58 Jan. 29	54 Jan. 23	50 Jan. 18	46 Jan. 14
25	65 Mar. 23	65 Mar. 12	63 Mar. 1	61 Feb. 19	58 Feb. 11	55 Feb. 4	52 Jan. 28	48 Jan. 23	44 Jan. 19
30	60 Mar. 23	60 Mar. 14	59 Mar. 4	57 Feb. 23	54 Feb. 15	52 Feb. 8	49 Feb. 2	45 Jan. 28	42 Jan. 23
35	55 Mar. 23	55 Mar. 15	54 Mar. 7	52 Feb. 27	50 Feb. 19	48 Feb. 12	45 Feb. 6	42 Feb. 1	39 Jan. 27
40	50 Mar. 23	50 Mar. 16	49 Mar. 8	48 Mar. 1	46 Feb. 22	44 Feb. 16	42 Feb. 9	39 Feb. 4	36 Jan. 30
45	45 Mar. 23	45 Mar. 17	44 Mar. 10	43 Mar. 3	42 Feb. 24	40 Feb. 18	38 Feb. 12	35 Feb. 7	33 Feb. 1
50	40 Mar. 23	40 Mar. 17	39 Mar. 11	38 Mar. 4	37 Feb. 26	36 Feb. 20	34 Feb. 14	32 Feb. 9	29 Feb. 4
55	35 Mar. 23	35 Mar. 18	34 Mar. 12	34 Mar. 6	33 Feb. 28	31 Feb. 22	30 Feb. 16	28 Feb. 11	26 Feb. 6
60	30 Mar. 23	30 Mar. 18	29 Mar. 12	29 Mar. 7	28 Mar. 1	27 Feb. 23	26 Feb. 18	24 Feb. 12	23 Feb. 7
65	25 Mar. 23	25 Mar. 18	25 Mar. 13	24 Mar. 7	23 Mar. 2	23 Feb. 24	21 Feb. 19	20 Feb. 14	19 Feb. 9
70	20 Mar. 23	20 Mar. 19	20 Mar. 13	19 Mar. 8	19 Mar. 3	18 Feb. 25	17 Feb. 20	16 Feb. 15	15 Feb. 10
75	15 Mar. 23	15 Mar. 19	15 Mar. 13	14 Mar. 8	14 Mar. 3	14 Feb. 26	13 Feb. 21	12 Feb. 16	11 Feb. 10
80	10 Mar. 23	10 Mar. 19	10 Mar. 14	10 Mar. 9	9 Mar. 3	9 Feb. 26	9 Feb. 21	8 Feb. 16	8 Feb. 11
85	5 Mar. 23	5 Mar. 19	5 Mar. 14	5 Mar. 9	5 Mar. 4	5 Feb. 27	4 Feb. 21	4 Feb. 16	4 Feb. 11
90	0 Mar. 23	0 Mar. 19	0 Mar. 14	0 Mar. 9	0 Mar. 4	0 Feb. 27	0 Feb. 22	0 Feb. 17	0 Feb. 11

45	50	55	60	65	70	75	80	85	90
45	40	35	30	25	20	15	10	5	0
Dec. 28	Dec. 27	Dec. 26	Dec. 26	Dec. 25	Dec. 25	Dec. 24	Dec. 24	Dec. 23	Dec. 23
44	39	34	29	25	20	15	10	5	0
Jan. 2	Dec. 31	Dec. 30	Dec. 29	Dec. 27	Dec. 26	Dec. 25	Dec. 25	Dec. 24	Dec. 23
43	38	34	29	24	19	14	10	5	0
Jan. 6	Jan. 4	Jan. 2	Dec. 31	Dec. 30	Dec. 28	Dec. 27	Dec. 25	Dec. 24	Dec. 23
42	37	33	28	23	19	14	9	5	0
Jan. 11	Jan. 8	Jan. 5	Jan. 3	Jan. 1	Dec. 30	Dec. 28	Dec. 26	Dec. 24	Dec. 23
40	36	31	27	23	18	14	9	5	0
Jan. 15	Jan. 12	Jan. 8	Jan. 6	Jan. 3	Jan. 1	Dec. 29	Dec. 27	Dec. 25	Dec. 23
38	34	30	26	21	17	13	9	4	0
Jan. 19	Jan. 15	Jan. 11	Jan. 8	Jan. 5	Jan. 2	Dec. 30	Dec. 28	Dec. 25	Dec. 23
35	32	28	24	20	16	12	8	4	0
Jan. 22	Jan. 18	Jan. 14	Jan. 10	Jan. 7	Jan. 4	Jan. 1	Dec. 29	Dec. 26	Dec. 23
33	29	26	23	19	15	11	8	4	0
Jan. 25	Jan. 20	Jan. 16	Jan. 12	Jan. 9	Jan. 5	Jan. 2	Dec. 29	Dec. 26	Dec. 23
30	27	24	21	17	14	11	7	4	0
Jan. 27	Jan. 23	Jan. 18	Jan. 14	Jan. 10	Jan. 6	Jan. 3	Dec. 30	Dec. 26	Dec. 23
27	24	22	19	16	13	10	6	3	0
Jan. 30	Jan. 25	Jan. 20	Jan. 16	Jan. 12	Jan. 8	Jan. 4	Dec. 31	Dec. 27	Dec. 23
24	22	19	17	14	11	9	6	3	0
Feb. 1	Jan. 27	Jan. 22	Jan. 17	Jan. 13	Jan. 9	Jan. 4	Dec. 31	Dec. 27	Dec. 23
21	19	17	14	12	10	7	5	2	0
Feb. 2	Jan. 28	Jan. 23	Jan. 19	Jan. 14	Jan. 9	Jan. 5	Jan. 1	Dec. 27	Dec. 23
17	16	14	12	10	8	6	4	2	0
Feb. 4	Jan. 30	Jan. 25	Jan. 20	Jan. 15	Jan. 10	Jan. 6	Jan. 1	Dec. 27	Dec. 23
14	13	11	10	8	7	5	3	2	0
Feb. 5	Jan. 31	Jan. 26	Jan. 21	Jan. 16	Jan. 11	Jan. 6	Jan. 1	Dec. 28	Dec. 23
11	10	9	7	6	5	4	3	1	0
Feb. 5	Jan. 31	Jan. 26	Jan. 21	Jan. 16	Jan. 11	Jan. 6	Jan. 2	Dec. 28	Dec. 23
7	6	6	5	4	3	3	2	1	0
Feb. 6	Feb. 1	Jan. 27	Jan. 22	Jan. 17	Jan. 12	Jan. 7	Jan. 2	Dec. 28	Dec. 23
4	3	3	2	2	2	1	1	0	0
Feb. 6	Feb. 1	Jan. 27	Jan. 22	Jan. 17	Jan. 12	Jan. 7	Jan. 2	Dec. 28	Dec. 23
0	0	0	0	0	0	0	0	0	0
Feb. 6	Feb. 1	Jan. 27	Jan. 22	Jan. 17	Jan. 12	Jan. 7	Jan. 2	Dec. 28	Dec. 23

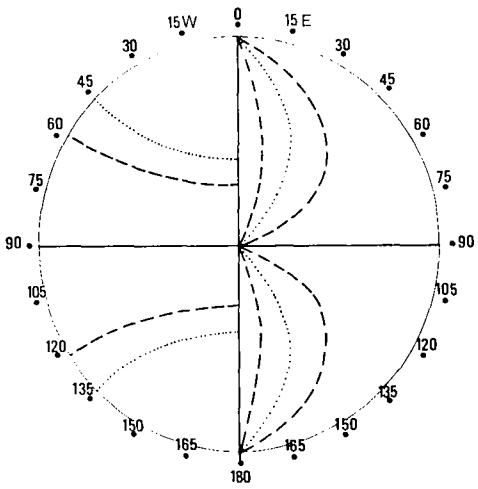

Fig. 4.

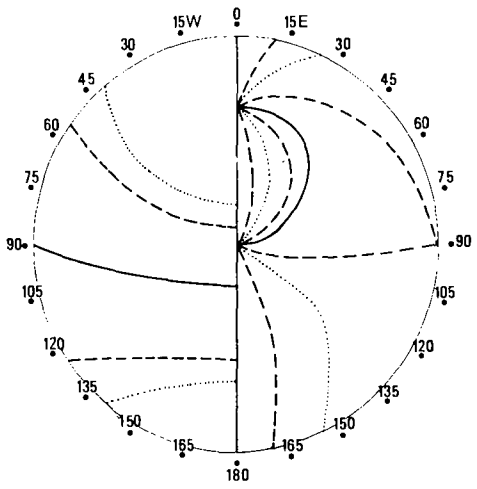

Fig. 5.

Fig. 4. – The radiation and polarization pattern curves drawn on the overlays for $\delta_a = 0°$. Because of the bilateral symmetry, both the patterns are shown: radiation pattern on the l.h.s. (——— $\vartheta = 90°$, $\eta_\vartheta = 1$; — — — $\vartheta = 57.23°$, $\eta_\vartheta = \frac{1}{2}$; · · · $\vartheta = 45°$, $\eta_\vartheta = \frac{1}{4}$), polarization pattern on the r.h.s. (——— $\varphi = 0°$, $\eta_\varphi = 1$; — — — $\varphi = \pm 22.5°$, $\eta_\varphi = \frac{1}{2}$; · · · $\varphi = 45°$, $\eta_\varphi = 0°$).

Fig. 5. – The radiation and polarization pattern curves drawn on the overlays for $\delta_a = 22.5°$. Because of the bilateral symmetry, both the patterns are shown: radiation pattern on the l.h.s. (——— $\vartheta = 90°$, $\eta_\vartheta = 1$; — — — $\vartheta = 57.23°$, $\eta_\vartheta = \frac{1}{2}$; · · · $\vartheta = 45°$, $\eta_\vartheta = \frac{1}{4}$), polarization pattern on the r.h.s. (— — — $\varphi = 0°$, $\eta_\varphi = 1$; — — — $\varphi = \pm 22.5°$, $\eta_\varphi = \frac{1}{2}$; · · · $\varphi = 45°$, $\eta_\varphi = 0°$).

corresponding to

$$\vartheta = 90°,\ 57.23°,\ 45°. \tag{12c}$$

c_2) *Polarization pattern overlay* (PPO) with lines of equation

$$\eta_\varphi = \cos^2 2\varphi = \text{const} \tag{13a}$$

with

$$\eta_\varphi = 1,\ \tfrac{1}{2},\ 0,\ \tfrac{1}{2} \tag{13b}$$

corresponding to

$$\varphi = 0°,\ 22.5°,\ 45°,\ 67.5°. \tag{13c}$$

A scale (S_0) in degrees from 180° E to 180° W is marked along the edge

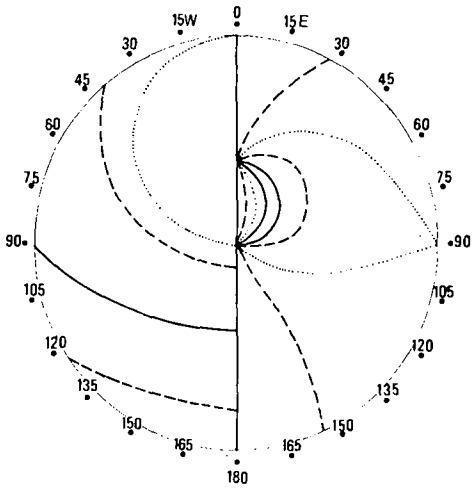

Fig. 6.

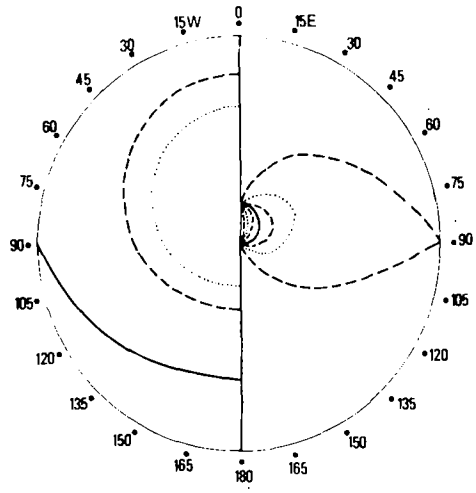

Fig. 7.

Fig. 6. – The radiation and polarization pattern curves drawn on the overlays for $\delta_a = 45°$. Because of the bilateral symmetry, both the patterns are shown: radiation pattern on the l.h.s. (——— $\vartheta = 90°$, $\eta_\vartheta = 1$; — — — $\vartheta = 57.23°$, $\eta_\vartheta = \frac{1}{2}$; · · · $\vartheta = 45°$, $\eta_\vartheta = \frac{1}{4}$), polarization pattern on the r.h.s. (——— $\varphi = 0°$, $\eta_\varphi = 1$; — — — $\varphi = \pm 22.5°$, $\eta_\varphi = \frac{1}{2}$; · · · $\varphi = 45°$, $\eta_\varphi = 0°$).

Fig. 7. – The radiation and polarization pattern curves drawn on the overlays for $\delta_a = 67.5°$. Because of the bilateral symmetry, both the patterns are shown: radiation pattern on the l.h.s. (— — — $\vartheta = 90°$, $\eta_\vartheta = 1$; — — — $\vartheta = 57.23°$, $\eta_\vartheta = \frac{1}{2}$; · · · $\vartheta = 45°$, $\eta_\vartheta = \frac{1}{4}$), polarization pattern on the r.h.s. (——— $\varphi = 0°$, $\eta_\varphi = 1$; — — — $\varphi = \pm 22.5°$, $\eta_\varphi = \frac{1}{2}$; · · · $\varphi = 45°$, $\eta_\varphi = 0°$).

of each overlay. The zero of the scale is at the point of crossing with the symmetry axis d (intersection with the vertical plane containing z) on the side of z. It is used in connection with different time scales: Local Time or Universal Time.

Local Time: the *zero* of S_0 is set at

$$\alpha_a' = \alpha_a - \text{long} = \arccos\left[-\operatorname{tg}(\text{lat}) \cdot \operatorname{tg} \delta_a\right] \tag{14}$$

read on S_h, measured from September, 23.

Universal Time: the value of the longitude of the CRA, read on S_0, is set in correspondence of the value of α_a' given by (14), read on S_h.

d) Two formulae providing the right ascension α_a' and the declination δ_a of the direction of the CRA axis. The first is equality (14) given above, while the second is

$$\delta_a = \arcsin\left[\cos \varrho \cdot \cos(\text{lat})\right], \tag{15}$$

where ϱ is the azimuthal angle defined as the angle between the local meridian and $\hat{z}$ ($\varrho = 90°$ for $\hat{z}$ in the East-West direction).

The α_a' obtained from (14) gives the angle of setting of the overlay (C_1) and (C_2) with respect to the holder as a function of the latitude of the CRA and the value of ϱ. The values of δ_a and α_a' *vs.* the values of ϱ and latitude are given in table II.

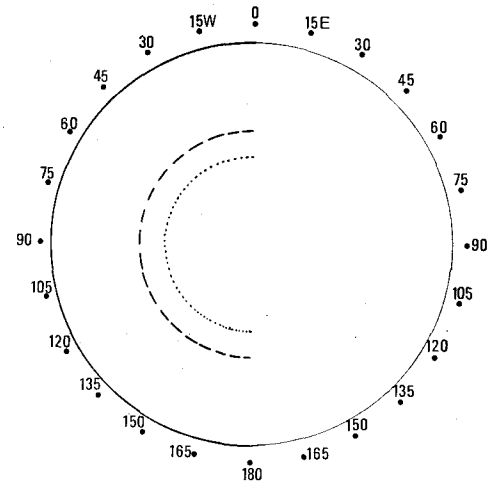

Fig. 8. – The radiation and polarization pattern curves drawn on the overlays for $\delta_a = 90°$. ——— $\vartheta = 90°$, $\eta_\vartheta = 1$; — — — $\vartheta = 57.23°$, $\eta_\vartheta = \frac{1}{2}$; · · · $\vartheta = 45°$, $\eta_\vartheta = \frac{1}{4}$. All points have $\varphi = 0$.

2·2. *Example of use of the astrolabe.* – Suppose we have a CRA in a certain location, for example Rome, with a certain azimuthal orientation, for example $\varrho = 90°$, and we ask its response to signals from a few sources at a preassigned value of the Local Time, for example January 16, 17 h 45 min.

The operator proceeds as follows:

1) He chooses the RPO and PPO corresponding to the value of δ_a deduced from table II for the chosen station and the value of ϱ corresponding to the chosen orientation of the CRA.

2) He places the two overlays on the holder with the marks drawn near their edges in correspondence of January 0 on S_h.

3) He screws the *lock knob* at the centre of the astrolabe.

The instrument is now *ready* for any operation (in Local Time) concerning the chosen station.

4) The holder is rotated until the local time marked on the scale S_b coincides with the day of the year marked on scale S_h.

The operator can now read the astrolabe: the RPO allows an estimate of the reduction factor η_ϑ introduced by the CRA of the energy carried by unpolarized waves due to sources located in any point of the sky; the PPO provides a similar estimate about the reduction η_φ due to the angle of polarization of linearly polarized radiation originating from sources located in any point of the sky.

3. – The construction of the astrolabe.

The map of the sky appearing on the base of the astrolabe is obtained by stereographic projection, *i.e.* by projecting the celestial sphere from the South pole on a plane parallel to the celestial equator (fig. 9). The main reason for the choice of this projection is the following well-known property: any circle on the celestial sphere is projected into a circle, the radius of which becomes infinite whenever the celestial circle crosses the South pole.

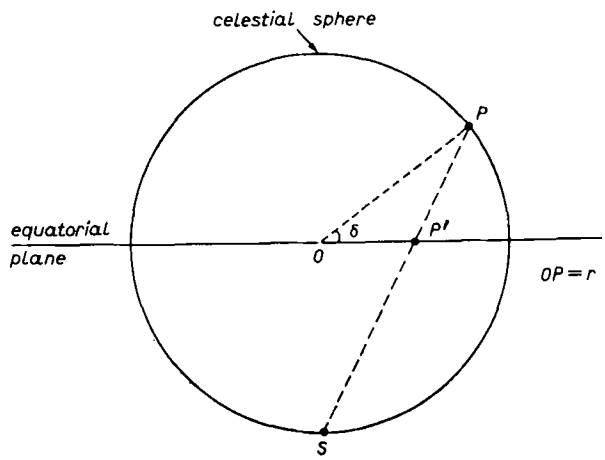

Fig. 9. – Stereographic-projection scheme.

On the contrary, the complications encountered by this method for the celestial hemisphere containing the projection pole are irrelevant in our case, since we use *only* the opposite hemisphere.

The basic equation of stereographic projection is (fig. 9)

$$OP' = r \operatorname{tg} \frac{90° - \delta}{2} . \tag{16}$$

The direction of the CRA's axis $\hat{z}$ is fixed with respect to the Earth and forms the angle δ_a (= declination) with the celestial equatorial plane. The angle

δ_a remains *constant* during the motions of rotation and revolution of the Earth (we neglect, as usual, the variations of δ_a due to precession). For a complete description of the motion of the intersection of the direction $\hat{z}$ with the plane of the map, we need a second angle α_a ($\equiv$ right ascension) which gives the position at Greenwich sideral time $t_s = 0$. We have

$$\delta_a(t_s = 0) = \arcsin [\cos \varrho \cdot \cos (\text{lat})], \tag{17}$$

$$\alpha_a(t_s = 0) = \text{long} + \arccos [- \operatorname{tg} (\text{lat}) \cdot \operatorname{tg} \delta_a]. \tag{18}$$

Notice that, in constrast to

$$\delta_a(t_s) = \delta_a(0), \tag{19}$$

we have

$$\alpha_a(t_s) = \alpha_a(0) + t_s(\text{in degrees}). \tag{20}$$

Because of (19) the curves corresponding to eqs. (12*a*) and (13*a*) are completely defined by the value of δ_a, apart from a rotation around the pole corresponding to (20), *i.e.* the variation of α_a with the Sideral Time t_s with the appropriate initial conditions.

Notice that all curves (12*a*) and (13*a*) have at least one bilateral symmetry axis (*d*) (two for $\delta_a = 0$) which passes through the pole at an angle α_a on the scale S_h.

Radiation pattern curves. Equation (12*a*), expressed in terms of the equatorial co-ordinates (α, δ), becomes

$$\eta_\vartheta(\alpha, \delta; \alpha_a, \delta_a) = \{1 - [\cos \delta \cdot \cos \delta_a \cdot \cos (\alpha - \alpha_a) + \sin \delta \cdot \sin \delta_a]^2\}^2, \tag{21}$$

where (α_a, δ_a) define the direction of the CRA's axis. The reduction factor takes its maximum value (= 1) along the maximum circle perpendicular to the CRA's axis. It is equal to an assigned constant value (between 0 and 1) along two circles, equal to each other, parallel and placed symmetrically with respect to the maximum circle defined above. In the stereographic projection these circles remain either circles with the centre on the axis *d*, or straight lines perpendicular to *d* (fig. 10).

For the maximum circle ($r = OF$) we have

$$\begin{cases} OA' = r \operatorname{tg} \dfrac{\delta_a}{2}, \\ OB' = r \operatorname{tg} \dfrac{180 - \delta_a}{2}. \end{cases} \tag{22}$$

For a circle of « height » β ($\equiv \widehat{COA}$) with respect to the maximum circle (fig. 10) we have

$$(23a) \qquad \begin{cases} OC' = r \operatorname{tg} \dfrac{\delta_a - \beta}{2} \\ OD' = r \operatorname{tg} \dfrac{180 - (\delta_a + \beta)}{2} \end{cases} \qquad \text{for } \beta > \delta_a - 90 ,$$

$$(23b) \qquad \begin{cases} OC' = r \operatorname{tg} \dfrac{180 - (\delta_a - \beta)}{2} \\ OD' = r \operatorname{tg} \dfrac{180 - (\delta_a + \beta)}{2} \end{cases} \qquad \text{for } \beta < \delta_a - 90 .$$

Notice that $\beta > 0$ means the hemisphere opposite to the projection pole, $\beta < 0$ the hemisphere containing the pole.

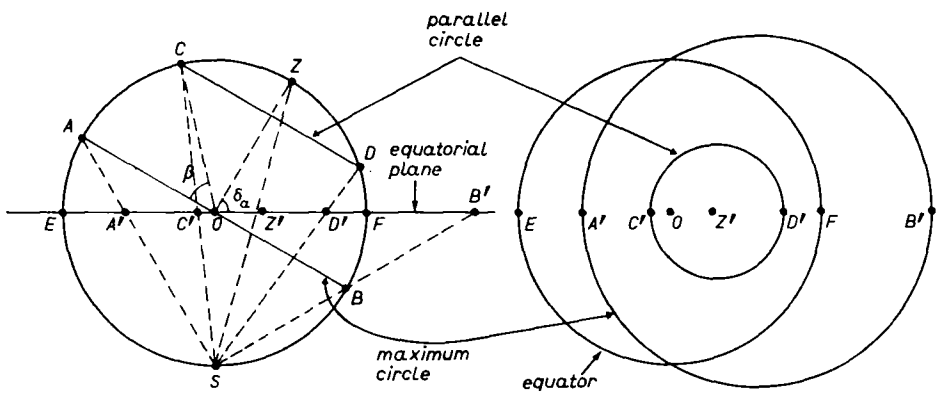

Fig. 10. – Stereographic projection of circles on the sphere.

Polarization pattern curves. The variables involved are 1) the equatorial co-ordinates (α_a, δ_a) of the CRA, 2) the direction of the incoming wave (α, δ) and 3) the direction of its polarization (α_p, δ_p). The last direction forms the angle ψ with the celestial meridian of the source (α, δ). In terms of these quantities eq. (13*a*) becomes (appendix)

$$(24) \qquad \eta_\varphi = [2(\cos \delta_p \cdot \cos \xi \cdot \cos (\alpha_p - \zeta) + \sin \delta_p \cdot \sin \xi)^2 - 1]^2 ,$$

where

$$(25) \qquad \zeta = \operatorname{arctg} \frac{\cos \delta_a \cdot \operatorname{tg} \delta - \sin \delta_a \cdot \cos \delta}{\sin \delta_a \cdot \sin \alpha} ,$$

$$(26) \qquad \xi = \operatorname{arctg} \left(- \frac{\cos \zeta}{\operatorname{tg} \delta_a} \right)$$

and α_p, δ_p can be expressed in terms of α, δ and ψ

$$(27) \qquad \begin{cases} \alpha_p = \alpha + \arccos(-\operatorname{tg}\delta \cdot \operatorname{tg}\delta_p), \\ \delta_p = \arcsin(\cos\psi \cdot \cos\delta). \end{cases}$$

* * *

I want to acknowledge Prof. E. AMALDI for his encouragement and the many advices; I am also indebted to Mr. E. SERRANI for the practical realization of the prototype.

APPENDIX A

Derivation of eqs. (24) to (27).

In equatorial co-ordinates we have

$$(A.1) \qquad \hat{z} = (0, \delta_a),$$

$$(A.2) \qquad \hat{w} = (\alpha_w, \delta_w),$$

where we have set $\alpha_a = 0$ without loss of generality because of the symmetry of rotation with respect to α_a.

In these co-ordinates the angle between two versors (α_1, δ_1), (α_2, δ_2) is

$$(A.3) \qquad \cos\varrho_{12} = \cos\delta_1 \cdot \cos\delta_2 \cdot \cos(\alpha_1 - \alpha_2) + \sin\delta_1 \cdot \sin\delta_2 .$$

Therefore, the maximum circle orthogonal to a versor (α, δ) has the equation

$$(A.4) \qquad \cos(\varphi - \alpha) = -\operatorname{tg}\vartheta \cdot \operatorname{tg}\delta ,$$

where (φ, ϑ) are the co-ordinates of a variable point on the celestial sphere. Thus the versor (ζ, ξ) orthogonal to $\hat{z}$ and $\hat{w}$ satisfies the equations

$$(A.5) \qquad \begin{cases} \cos\zeta = -\operatorname{tg}\xi \cdot \operatorname{tg}\delta_a , \\ \cos(\zeta - \alpha) = -\operatorname{tg}\xi \cdot \operatorname{tg}\delta . \end{cases}$$

From these expressions we derive

$$(A.6) \qquad \operatorname{tg}\xi = -\frac{\cos\zeta}{\operatorname{tg}\delta_a},$$

$$(A.7) \qquad \cos\zeta \cdot \cos\alpha + \sin\zeta \cdot \sin\alpha = \frac{\operatorname{tg}\delta}{\operatorname{tg}\delta_a}\cos\zeta ,$$

$$(A.8) \qquad \operatorname{tg}\zeta = \frac{\cos\delta_a \cdot \operatorname{tg}\delta - \sin\delta_a \cdot \cos\alpha}{\sin\delta_a \cdot \sin\alpha},$$

from which eqs. (25) and (26) are easily deduced.

The angle between $\hat{p}$ and (ζ, ξ) is $90° - \varphi$ (see fig. 1) and, therefore,

$$\cos(90 - \varphi) = \sin\varphi = \cos\delta_p \cdot \cos\xi \cdot \cos(\alpha_p - \zeta) + \sin\delta_p \cdot \sin\xi\,, \tag{A.9}$$

from which we deduce (eq. (24))

$$\cos^2 2\varphi = (1 - 2\sin^2\varphi)^2\,. \tag{A.10}$$

Furthermore, the tangent to the meridian at the point (α_w, δ_w) has the direction $(\alpha_w + 180, 90 - \delta_w)$. Therefore, the versors (α_p, δ_p) form with this direction the angle

$$\psi = \arccos[-\cos\delta_p \cdot \sin\delta_w \cdot \cos(\alpha_w - \alpha_p) + \sin\delta_p \cdot \cos\delta_w]\,. \tag{A.11}$$

The orthogonality of $\hat{p}$ and $\hat{w}$ is expressed by

$$\cos(\alpha_w - \alpha_p) = -\operatorname{tg}\delta_p \cdot \operatorname{tg}\delta_w\,, \tag{A.12}$$

which leads to

$$\cos\psi = \sin\delta_p \cdot (\sin\delta_w \cdot \operatorname{tg}\delta_w + \cos\delta_w) = \frac{\sin\delta_p}{\cos\delta_w}\,. \tag{A.13}$$

From eqs. (A.12) and (A.13) eqs. (27) are immediately obtained.

● RIASSUNTO

La risposta di un'antenna gravitazionale cilindrica dipende, oltre che dall'intensità dell'onda e dalla sensibilità dell'antenna, dall'angolo tra la direzione della sorgente e l'asse dell'antenna e dall'angolo di polarizzazione dell'onda. In quest'articolo si presenta uno strumento (astrolabio gravitazionale) che può calcolare approssimativamente la parte angolare della risposta. Con esso si possono facilmente calcolare la zona del cielo verso cui è « diretta » una data antenna a un dato istante, l'angolo di polarizzazione che è meglio « ricevuto » e si possono risolvere molti simili problemi.

Аналоговый прибор для грубой локализации источников гравитационных волн.

Резюме (*). - - Отклик гравитационной цилиндрической антенны зависит, помимо значений интенсивности волны и чувствиельности антенны, от угла между направлением на источник и осью антенны и от угла поляризации волны. В этой статье предлагается прибор (гравитационная астролябия), который позволяет грубо определить угловую часть отклика. Результат задает зону неба, по направлению которой « направлена » антенна в определенное время, определяется угол поляризации и решается ряд аналогичных проблем.

(*) *Переведено редакцией.*